

# The Limited Multi-Label Projection Layer

Brandon Amos<sup>1\*</sup> Vladlen Koltun<sup>2</sup> J. Zico Kolter<sup>1,3</sup>

<sup>1</sup>Carnegie Mellon University

<sup>2</sup>Intel Labs

<sup>3</sup>Bosch Center for AI

## Abstract

We propose the Limited Multi-Label (LML) projection layer as a new primitive operation for end-to-end learning systems. The LML layer provides a probabilistic way of modeling multi-label predictions limited to having exactly  $k$  labels. We derive efficient forward and backward passes for this layer and show how the layer can be used to optimize the top- $k$  recall for multi-label tasks with incomplete label information. We evaluate LML layers on top- $k$  CIFAR-100 classification and scene graph generation. We show that LML layers add a negligible amount of computational overhead, strictly improve the model’s representational capacity, and improve accuracy. We also revisit the truncated top- $k$  entropy method as a competitive baseline for top- $k$  classification.

## 1 Introduction

Multi-label prediction tasks show up frequently in computer vision and language processing. Multi-label predictions can arise from a task being truly multi-label, as in language and graph generation tasks, or by turning a single-label prediction task into a multi-label prediction task that predicts a set of top- $k$  labels, for example. In high-dimensional cases, such as scene graph generation, annotating multi-label data is difficult and often results in datasets that have an incomplete labeling. In these cases, models are typically limited to predicting  $k$  labels and are evaluated on the recall, the proportion of known labels that are present in the model’s predicted set. As we will show later, the standard approaches of using a softmax or sigmoid functions are not ideal here as they have no way of allowing the model to capture labels that are unobserved.

In this report, we present the LML layer as a new way of modeling in multi-label settings where the model needs to make a prediction of exactly  $k$  labels. We derive how to efficiently implement and differentiate through LML layers in [Section 3](#). The LML layer has a probabilistic interpretation and can be trained with a standard maximum-likelihood approach that we show in [Section 4](#), where we also highlight applications to top- $k$  image classification and scene graph generation. We show experiments in [Section 5](#) on CIFAR-100 classification and scene graph generation.

## 2 Background and Related Work

Our work is motivated by the ubiquity of projections onto polytopes in machine learning. Here we review how the ReLU, sigmoid, and softmax operations can be interpreted as explicit closed-form solutions to a projection optimization problem and then go on to review related work on cardinality modeling, top- $k$  optimization, ranking-based loss functions, and scene graph generation.

### 2.1 Projections in Machine Learning

Projections onto polytopes are ubiquitous in machine learning. In this section, we motivate our contribution by reviewing how the ReLU, sigmoid, and softmax layers can be interpreted as explicit closed-form solutions to a projection optimization problem. Similar projections are also done onto

\*Work done while BA was an intern at Intel Labs.

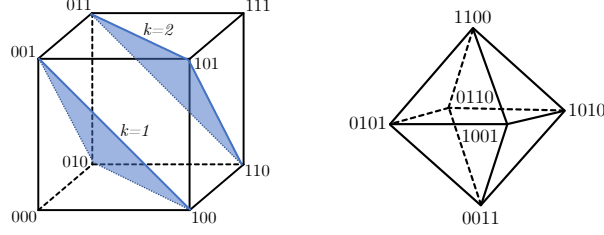


Figure 1: The LML polytope  $\mathcal{L}_{n,k}$  is the set of points in the unit  $n$ -hypercube with coordinates that sum to  $k$ .  $\mathcal{L}_{n,1}$  is the  $(n-1)$ -simplex. The  $\mathcal{L}_{3,1}$  and  $\mathcal{L}_{3,2}$  polytopes (triangles) are on the left in blue. The  $\mathcal{L}_{4,2}$  polytope (an octahedron) is on the right.

more complex polytopes such as the marginal polytope for structured inference [Niculae et al.] or the Birkhoff polytope for permutations [Adams and Zemel, Santa Cruz et al., Mena et al.].

**Theorem 1.** *The ReLU, defined by  $f(x) = \max\{0, x\}$ , can be interpreted as projecting a point  $x \in \mathbb{R}^n$  onto the non-negative orthant as*

$$f(x) = \operatorname{argmin}_y \frac{1}{2} \|x - y\|_2^2 \quad \text{s. t. } y \geq 0. \quad (1)$$

*Proof.* The usual solution can be obtained by looking at the KKT conditions of Equation (1). Introducing a dual variable  $\lambda \geq 0$  for the inequality constraint, the Lagrangian of Equation (1) is

$$L(y, \lambda) = \frac{1}{2} \|x - y\|_2^2 - \lambda^\top y. \quad (2)$$

The stationarity condition  $\nabla_y L(y^*, \lambda^*) = 0$  gives a way of expressing the primal optimal variable  $y^*$  in terms of the dual optimal variable  $\lambda^*$  as  $y^* = x + \lambda^*$ . Complementary slackness  $\lambda_i^*(x_i + \lambda_i^*) = 0$  shows that  $\lambda_i^* \in \{0, -x_i\}$ . Consider two cases:

- **Case 1:**  $x_i \geq 0$ . Then  $\lambda_i^*$  must be 0 since we require  $\lambda^* \geq 0$ . Thus  $y_i^* = x_i + \lambda_i^* = x_i$ .
- **Case 2:**  $x_i < 0$ . Then  $\lambda_i^*$  must be  $-x_i$  since we require  $y \geq 0$ . Thus  $y_i^* = x_i + \lambda_i^* = 0$ .

Combining these cases gives the usual solution of  $y^* = \max\{0, x\}$ .  $\square$

**Theorem 2.** *The sigmoid or logistic function, defined by  $f(x) = (1 + e^{-x})^{-1}$ , can be interpreted as projecting a point  $x \in \mathbb{R}^n$  onto the interior of the unit hypercube as*

$$f(x) = \operatorname{argmin}_{0 < y < 1} -x^\top y - H_b(y), \quad (3)$$

where  $H_b(y) = -(\sum_i y_i \log y_i + (1 - y_i) \log(1 - y_i))$  is the binary entropy function.

*Proof.* The usual solution can be obtained by looking at the first-order optimality condition of Equation (3). The domain of the binary entropy function  $H_b$  restricts us to  $0 < y < 1$  without needing to explicitly represent this as a constraint in the optimization problem. Let  $g(y; x) = -x^\top y - H_b(y)$  be the objective. The first-order optimality condition  $\nabla_y g(y^*; x) = 0$  gives us  $-x_i + \log y_i^* - \log(1 - y_i^*) = 0$  and thus  $y^* = (1 + e^{-x})^{-1}$ .  $\square$

**Theorem 3.** *The softmax, defined by  $f(x)_j = e^{x_j} / \sum_i e^{x_i}$ , can be interpreted as projecting a point  $x \in \mathbb{R}^n$  onto the interior of the  $(n-1)$ -simplex*

$$\Delta_{n-1} = \{p \in \mathbb{R}^n \mid 1^\top p = 1 \text{ and } p \geq 0\}$$

as

$$f(x) = \operatorname{argmin}_{0 < y < 1} -x^\top y - H(y) \quad \text{s. t. } 1^\top y = 1 \quad (4)$$

where  $H(y) = -\sum_i y_i \log y_i$  is the entropy function.

*Proof.* The usual solution can be obtained by looking at the KKT conditions of Equation (4). Introducing a scalar-valued dual variable  $\nu$  for the equality constraint, the Lagrangian is

$$L(y, \nu) = -x^\top y - H(y) + \nu(1^\top y - 1) \quad (5)$$

The stationarity condition  $\nabla_y L(y^*, \nu^*) = 0$  gives a way of expressing the primal optimal variable  $y^*$  in terms of the dual optimal variable  $\nu^*$  as

$$y_j^* = \exp\{x_j - 1 - \nu^*\}. \quad (6)$$

Putting this back into the equality constraint  $1^\top y^* = 1$  gives us  $\sum_i \exp\{x_i - 1 - \nu^*\} = 1$  and thus  $\nu^* = \log \sum_i \exp\{x_i - 1\}$ . Substituting this back into Equation (6) gives us the usual definition of  $y_j = e^{x_j} / \sum_i e^{x_i}$ .  $\square$

**Corollary 1.** *A temperature-scaled softmax scales the entropy term in the objective and the sparsemax [Martins and Astudillo] replaces the objective’s entropy penalty with a ridge section.*

## 2.2 Cardinality Potentials and Modeling

Cardinality potentials and modeling are a closely related line of work typically found in the structured prediction and constraint programming literature. Régin shows how to add constraints to models for worker scheduling. Tarlow et al., Globerson et al. propose ways of performing structured prediction with cardinality potentials, and Brukhim and Globerson propose a soft projection operation that integrate cardinality modeling into deep structured prediction architectures like SPENs [Belanger and McCallum]. In contrast to all of these methods, our projection and constraint is exact and can be integrated in the standard forward pass of a deep model outside of structured prediction. None of our experiments use structured prediction techniques and we instead do standard supervised learning of vanilla feedforward models that use our LML layer. In contrast to Brukhim and Globerson, we show that the backward pass of our soft projection can be exactly computed instead of unrolled as part of a structured prediction procedure.

## 2.3 Top- $k$ and Ranking-Based Loss Functions

There has been a significant amount of work on creating specialized loss functions for optimizing the model’s top- $k$  prediction error [Gupta et al., Li et al., a, Liu et al., Lapin et al., a, Liu et al., Lapin et al., b, Berrada et al.] and ranking error [Agarwal, Rudin, Boyd et al., Rakotomamonjy].

Most relevant to our contributions are the smooth top- $k$  loss functions discussed in Lapin et al. [b] and the Smooth SVM [Berrada et al.]. Among other loss functions, Lapin et al. [b] propose the truncated top- $k$  entropy loss, which we review in Section 2.3.1 and extend to cases when multiple ground-truth labels are present in Section 2.3.2.

In contrast to all of these methods, our approach does not hand-craft a loss function and instead puts the top- $k$  knowledge into the modeling part of the pipeline, which is then optimized as a likelihood maximization problem. We show in Section 5.2 that LML layers are competitive in the top- $k$  prediction task from Berrada et al..

### 2.3.1 Truncated Top- $k$ Entropy Derivation

This section reviews the truncated top- $k$  entropy derivation from Section 2.5 of Lapin et al. [b]. We start with the standard likelihood

$$P(y | x) = \frac{\exp\{f_y(x)\}}{\sum_j \exp\{f_j(x)\}} \quad (7)$$

and then consider the negative log-likelihood

$$\begin{aligned} -\log P(y | x) &= -\log \frac{\exp\{f_y(x)\}}{\sum_j \exp\{f_j(x)\}} \\ &= \log \frac{\sum_j \exp\{f_j(x)\}}{\exp\{f_y(x)\}} \\ &= \log \left( 1 + \sum_{j \neq y} \exp\{f_j(x) - f_y(x)\} \right) \end{aligned} \quad (8)$$

Truncating the index set of the last sum gives the truncated top- $k$  entropy loss

$$\log \left( 1 + \sum_{j \in \mathcal{J}_y} \exp\{f_j(x) - f_y(x)\} \right) \quad (9)$$

where  $\mathcal{J}_y$  are the indices of the  $m - k$  smallest components of  $(f_j(x))_{j \neq y}$ . This loss is small whenever the top- $k$  error is zero.

### 2.3.2 Multi-Label Truncated Top- $k$ Entropy Derivation

The truncated top- $k$  entropy loss from [Lapin et al. \[b\]](#) is a competitive and simple loss function for optimizing the model's top- $k$  predictions in single-label classification tasks. In this section, we show how it can be extended to optimizing the top- $k$  predictions in multi-label classification tasks, such as scene graph generation.

We start by making an independence assumption between the observed labels and decomposing the likelihood as

$$P(Y | x) = \prod_i P(Y_i | x). \quad (10)$$

Then, we can assume the likelihood of each label is obtained with a softmax as

$$P(Y_i | x) = \frac{\exp\{f_{y_i}(x)\}}{\sum_j \exp\{f_j(x)\}}. \quad (11)$$

We note that in general, maximum-likelihood estimation of the form [Equation \(11\)](#) will never achieve perfect likelihood as the softmax restricts the likelihoods over all of the labels. However following the approach from [Lapin et al. \[b\]](#), we can rearrange the terms of the negative log-likelihood and truncate parts of to obtain a reasonable loss function.

$$\begin{aligned} -\log P(Y | x) &= -\sum_i \log \frac{\exp\{f_{y_i}(x)\}}{\sum_j \exp\{f_j(x)\}} \\ &= \sum_i \log \frac{\sum_j \exp\{f_j(x)\}}{\exp\{f_{y_i}(x)\}} \\ &= \sum_i \log \left( 1 + \sum_{j \neq y_i} \exp\{f_j(x) - f_{y_i}(x)\} \right) \end{aligned} \quad (12)$$

Truncating the index set of the last sum gives the multi-label truncated top- $k$  entropy loss

$$\sum_i \log \left( 1 + \sum_{j \in \mathcal{J}_y} \exp\{f_j(x) - f_{y_i}(x)\} \right) \quad (13)$$

where  $\mathcal{J}_y$  are the indices of the  $m - k$  smallest components of  $(f_j(x))_{j \notin y}$ . This loss is small whenever the top- $k$  recall is zero.

## 2.4 Scene Graph Generation

Scene graph generation is the task of generating a set of objects and relationships between them from an input image and has been extensively studied recently [[Johnson et al.](#), [Yang et al.](#), [Plummer et al.](#), [Liang et al.](#), [Raposo et al.](#), [Newell and Deng](#), [Xu et al.](#), [Li et al.](#), [b](#), [Herzig et al.](#), [Zellers et al.](#), [Woo et al.](#)]. Most relevant to our work are the methods that score all of the possible relationships between objects and select the top-scoring relationships [[Xu et al.](#), [Li et al.](#), [b](#), [Herzig et al.](#), [Woo et al.](#)]. These methods include the near-state-of-the-art Neural Motifs model [[Zellers et al.](#)] that generates a scene graph by creating object- and edge-level contexts.

We propose a way of improving the relationship prediction portion of methods that fully enumerate all of the possible relationships, and we empirically demonstrate that this improves the representational capacity of Neural Motifs.

---

**Module 1** The Limited Multi-Label Projection Layer

---

**Input:**  $x \in \mathbb{R}^n$ **Forward Pass***(Described in [Section 3.1](#))*

- 1: Compute  $\nu^*$  with [Algorithm 1](#)
- 2: **return**  $y^* = \sigma(x + \nu^*)$

**Backward Pass***(Described in [Section 3.2](#))*

- 1:  $h = (y^*)^{-1} + (1 - y^*)^{-1}$
  - 2:  $d_\nu = (1^\top h^{-1})^{-1} h^{-\top} (\nabla_{y^*} \ell)$
  - 3:  $d_y = h^{-1} \circ (d_\nu - \nabla_{y^*} \ell)$
  - 4: **return**  $\nabla_x \ell = -d_y$
- 

### 3 The Limited Multi-Label Projection Layer

We propose the *Limited Multi-Label projection layer* as a way of projecting onto the set of points in the unit  $n$ -hypercube with coordinates that sum to exactly  $k$ . This space can be represented as a polytope, which we define as the  $(n, k)$ -*Limited Multi-Label polytope*

$$\mathcal{L}_{n,k} = \{p \in \mathbb{R}^n \mid 0 \leq p \leq 1 \text{ and } 1^\top p = k\}.$$

When  $k = 1$ , the LML polytope is the  $(n - 1)$ -simplex. Notationally, if  $n$  is implied by the context we will leave it out and write  $\mathcal{L}_k$ . [Figure 1](#) shows three low-dimensional examples of this polytope.

We consider projections onto the interior of the LML polytope of the form

$$\Pi_{\mathcal{L}_k}(x) = \underset{0 < y < 1}{\operatorname{argmin}} \quad -x^\top y - H_b(y) \quad \text{s. t.} \quad 1^\top y = k \quad (14)$$

where  $H_b(y) = -\sum_i y_i \log y_i + (1 - y_i) \log(1 - y_i)$  is the binary entropy function. The entropy-based regularizer in the objective helps prevent sparsity in the gradients of this projection, which is important for learning and the same reason it is useful in the softmax. We note that other projections could be done by changing the regularizer or by scaling the entropy term with a temperature parameter. The following is one useful property of the LML projection when  $x$  is the output of a function such as a neural network.

**Proposition 1.**  $\Pi_{\mathcal{L}_k}(x)$  preserves the (magnitude-based) order of the coordinates of  $x$ .

The intuition is that  $\Pi_{\mathcal{L}_k}(x)$  can be decomposed to applying a monotonic transformation to each element of  $x$ , which we show in [Equation \(15\)](#). Thus, this preserves the (magnitude-based) ordering of  $x$ .

The LML projection layer does not have an explicit closed-form solution like the layers discussed in [Section 2.1](#), despite the similarity to the softmax layer. We show how to efficiently solve the optimization problem for the forward pass in [Section 3.1](#) and how to backpropagate through the LML projection in [Section 3.2](#) by implicitly differentiating the KKT conditions. [Module 1](#) summarizes the implementation of the layer.

---

**Algorithm 1** Bracketing method to find  $g(\nu) = 0$ 


---

**Input:**  $x \in \mathbb{R}^n$

**Parameters:**  $d$ : the number of per-iteration samples

$\Delta$ : the saturation offset

- 1: Initialize  $\nu_\ell = -\pi(x)_k - \Delta$  and  $\nu_u = -\pi(x)_{k+1} + \Delta$
  - 2: **while**  $|\nu_\ell - \nu_u| > \epsilon$  **do**
  - 3:     Sample  $\nu_{1:d}$  linearly from the interval  $[\nu_\ell, \nu_u]$
  - 4:      $g_{1:d} = (g(\nu_i))_{i=1}^d$   $\triangleright$  Ideally parallelized
  - 5:      $\triangleright$  Return the corresponding  $\nu_i$  early if any  $g_i = 0$
  - 6:      $i_\ell = \max\{i \mid g_i < 0\}$  and  $i_u = i_\ell + 1$
  - 7:      $\nu_\ell = \nu_{i_\ell}$  and  $\nu_u = \nu_{i_u}$
  - 8: **end while**
  - 9: **return**  $(\nu_\ell + \nu_u)/2$
- 

### 3.1 Efficiently computing the LML projection

The LML projection in Equation (14) is a convex and constrained optimization problem. In this section we propose an efficient way of solving it that is GPU-amenable.

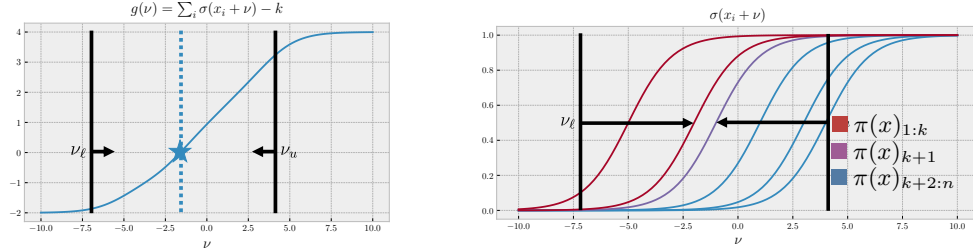


Figure 2: Example of finding the optimal dual variable  $\nu$  with  $x \in \mathbb{R}^6$  and  $k = 2$  by solving the root-finding problem  $g(\nu) = 0$  in Equation (16), which is shown on the left. The right shows the decomposition of the individual logistic functions that contribute to  $g(\nu)$ . We show the initial lower and upper bounds described in Section 3.1.1.

Introducing a dual variable  $\nu \in \mathbb{R}$  for the constraint  $k - 1^\top y = 0$ , the Lagrangian of Equation (14) is

$$L(y, \nu) = -x^\top y - H_b(y) + \nu(k - 1^\top y),$$

where we unconventionally negate the equality constraint to make analyzing  $g(\nu)$  easier. Differentiating this gives

$$\nabla_y L(y, \nu) = -x + \log \frac{y}{1-y} - \nu$$

and the first-order optimality condition  $\nabla_y L(y^*, \nu^*) = 0$  gives

$$y^* = \sigma(x + \nu^*) \tag{15}$$

where  $\sigma$  is the logistic function. To find the optimal dual variable  $\nu^*$ , we can substitute Equation (15) into the constraint

$$g(\nu) \triangleq 1^\top \sigma(x + \nu) - k = 0. \tag{16}$$

Thus the LML projection can be computed by solving  $g(\nu) = 0$  for the optimal dual variable and then using Equation (15) for the projection.

#### 3.1.1 Solving $g(\nu) = 0$

$g(\nu) = 0$  is a scalar-valued root-finding problem of a differentiable, continuous, non-convex function that is monotonically increasing. Despite the differentiability, we advocate for solving  $g(\nu) = 0$  with a *bracketing method* that maintains an interval of lower and upper bounds around the solution  $\nu^*$  and is amenable to parallelization, instead of a Newton method that would use the derivative information but is not as amenable to parallelization. Our method generalizes the bisection bracketing method by

sampling  $g(\nu)$  for  $d$  values of  $\nu$  per iteration instead of a single point. On the GPU by default, we sample  $d = 100$  points in parallel for each iteration, which usually reaches machine epsilon in less than 10 iterations, and on the CPU we sample  $d = 10$  points. We present our bracketing method in [Algorithm 1](#) and show an example of  $g(\nu)$  and the component functions in [Figure 2](#).

The initial lower bound  $\nu_\ell$  and upper bound  $\nu_u$  on the root can be obtained by observing that  $g(\nu)$  takes a sum of logistic functions that are offset by the entries of  $x \in \mathbb{R}^n$  as  $\sigma(x_j + \nu)$ . With high probability, we can use the saturated areas of the logistic functions to construct the initial bounds.

Let  $\pi(x)$  sort  $x \in \mathbb{R}^n$  in descending order so that

$$\pi(x)_1 \geq \pi(x)_2 \geq \dots \geq \pi(x)_n$$

and  $\Delta$  be a sufficiently large offset that causes the sigmoid units to saturate. We use  $\Delta = 7$  in all of our experiments.

Use  $\nu_\ell = -\pi(x)_k - \Delta$  for the **initial lower bound**. This makes  $\sigma(x_j + \nu_\ell) \approx 0$  for  $x_j \in \pi(x)_{k,\dots,n}$  and  $0 < \sigma(x_j + \nu_\ell) < 1$  for  $x_j \in \pi(x)_{1,\dots,k-1}$ , and thus  $g(\nu_\ell) \leq -1 \leq 0$ .

Use  $\nu_u = -\pi(x)_{k+1} + \Delta$  for the **initial upper bound**. This makes  $\sigma(x_j + \nu_u) \approx 1$  for every  $x_j \in \pi(x)_{1,\dots,k+1}$  and thus  $g(\nu_u) \geq 1 \geq 0$ .

### 3.2 Backpropagating through the LML layer

Let  $y^* = \Pi_{\mathcal{L}_k}(x)$  be outputs of the LML layer from [Equation \(14\)](#). Integrating this layer into a gradient-based end-to-end learning system requires that we compute the derivative

$$\frac{\partial \ell}{\partial x} = \frac{\partial \ell}{\partial y^*} \frac{\partial y^*}{\partial x},$$

where  $\ell$  is a loss function. The LML projection  $\Pi_{\mathcal{L}_k}(x)$  does not have an explicit closed-form solution and we therefore cannot use an autodiff framework to compute the gradient  $\partial y^* / \partial x$ . We note that even though the solution can be represented as  $y^* = \sigma(x + \nu^*)$ , differentiating this form is still difficult because  $\nu^*$  is also a function of  $x$ . We instead implicitly differentiate the KKT conditions of [Equation \(14\)](#). Using the approach described, e.g., in OptNet [[Amos and Kolter](#)], we can solve the linear system

$$\begin{bmatrix} H & -1 \\ -1^\top & 0 \end{bmatrix} \begin{bmatrix} d_y \\ d_\nu \end{bmatrix} = - \begin{bmatrix} \nabla_{y^*} \ell \\ 0 \end{bmatrix} \quad (17)$$

where  $H = \nabla_y^2 L(y, \nu)$  is defined by  $H = \text{diag}(h)$  and

$$h = \frac{1}{y^*} + \frac{1}{1 - y^*}. \quad (18)$$

The system in [Equation \(17\)](#) can be solved analytically with

$$d_\nu = \frac{1}{1^\top h^{-1}} h^{-\top} (\nabla_{y^*} \ell) \quad \text{and} \quad d_y = h^{-1} \circ (d_\nu - \nabla_{y^*} \ell) \quad (19)$$

where  $\circ$  is the elementwise product and  $h^{-1}$  is the elementwise inverse. Finally, we have that  $\nabla_x \ell = -d_y$ .

## 4 Maximizing Top- $k$ Recall via Maximum Likelihood with The LML layer

In this section, we highlight one application of the LML layer for maximizing the top- $k$  recall. We consider a multi-label classification setting where the data has an incomplete (strict) subset of the true labels and we want to model the task by predicting a set of exactly  $k$  labels. This setting comes up in practice for predicting the top- $k$  labels in image classification and in predicting a set of  $k$  relationships in a graph for scene graph generation, which we discuss in [Sections 4.1](#) and [4.2](#), respectively.

Formally, we have samples  $(x_i, Y_i) \sim \mathcal{D}$  from some data generating process  $\mathcal{D}$  with features  $x_i \in \mathcal{X}_i$  and labels  $Y_i \subseteq Y_i^* \subseteq \mathcal{Y} \triangleq \{1, \dots, n\}$ , where  $Y_i^*$  are the ground-truth labels and  $Y_i$  are the *observed* labels. There is typically some  $k \ll n$  such that  $|Y_i^*| \leq k$  for all  $i$ . We will model this by predicting exactly  $k$  labels  $\hat{Y}_i \subseteq \{1, \dots, n\}$  where  $|\hat{Y}_i| = k$ .

---

**Algorithm 2** Maximizing top- $k$  recall via maximum likelihood with the LML layer.

---

**Model:**  $f_\theta : \mathcal{X} \rightarrow \mathbb{R}^n$

**Model Predictions:**  $\hat{Y}_i = \{j \mid f_\theta(x_i)_j \geq \pi(f_\theta(x_i))_k\}$

**Training Procedure:**

- 1: **while** unconverged **do**
- 2:   Sample  $(x_i, Y_i) \sim \mathcal{D}$
- 3:    $\hat{p} = \Pi_{\mathcal{L}_k}(f_\theta(x_i))$
- 4:   Update  $\theta$  with a gradient step  $\nabla_\theta \ell(Y_i, \hat{p})$  where

$$\ell(Y_i, \hat{p}) = - \sum_{j \in Y_i} \log \hat{p}_j$$

5: **end while**

---

The model's predictions should have high recall on the observed data, which for a single sample is defined by

$$\text{recall}(Y, \hat{Y}) = \frac{1}{|Y|} \sum_{j \in Y} \mathbb{I}[y_j \notin \hat{Y}],$$

where the Iverson bracket  $\mathbb{I}[P]$  is 1 if  $P$  is true and 0 otherwise. We note that the 0-1 error, defined as

$$\text{error}(Y, \hat{Y}) = \mathbb{I}[Y \neq \hat{Y}],$$

or smooth variants thereof, are not a reasonable proxy for the recall as it incorrectly penalizes the model when it makes a correct prediction  $\hat{Y}$  that is in the ground truth labels  $Y^*$  but not in the observation  $Y$ .

We will next use a probabilistic approach to motivate the use of LML layers for maximum recall. Given access to the ground-truth data in addition to the observation and assuming label independence, we could maximize the likelihood of a parametric model with

$$P(Y, Y^* \mid x) = \prod_{j \in \mathcal{Y}} P(j \in Y^* \mid x). \quad (20)$$

We can decompose  $P(Y, Y^* \mid x)$  as

$$\begin{aligned} P(Y, Y^* \mid x) &= \prod_{j \in Y^*} P(j \in Y^* \mid x) \prod_{j \in \mathcal{Y} - Y^*} P(j \notin Y^* \mid x) \\ &= \overbrace{\prod_{j \in Y} P(j \in Y^* \mid x)}^{\prod_{j \in Y^*} P(j \in Y^* \mid x)} \prod_{j \in Y^* - Y} P(j \in Y^* \mid x) \end{aligned}$$

The difficulty in modeling this problem given only the observed labels  $Y$  comes from not knowing which of the *unobserved* labels should be active or inactive. In the case when all  $|Y^*| = k$ , then the ground-truth labels can be interpreted as vertices of the LML polytope that have a value of 1 if the label is present and 0 otherwise. Thus, we can use a model that makes a prediction on the LML polytope  $f_\theta : \mathcal{X} \rightarrow \mathcal{L}_k$ . The outputs of this model  $\hat{p} = f_\theta(x)$  are then the likelihoods  $\hat{p}_j \triangleq P(j \in Y^* \mid x)$ . For example,  $f_\theta$  can be modeled with a standard deep feed-forward network with an LML layer at the end. The set of predicted labels can be obtained with

$$\hat{Y}(x) = \{j \mid f_\theta(x)_j \geq \pi(f_\theta(x))_k\},$$

breaking ties if necessary in the unlikely case that multiple  $f_\theta(x)_j = \pi(f_\theta(x))_k$ . We next state assumptions under which we can reason about maximum-likelihood solutions.

**Assumptions.** For the following, we assume that 1) in the infinite data setting, the ground-truth labels are able to be reconstructed from the observed labels (e.g. for a fixed feature, the observed labels are sampled from the ground-truth labels with a non-zero weight on each label), 2) there is no noise in the data generating process, 3) the true model is realizable and therefore maximizing the likelihoods can be done exactly, and 4) all  $|Y_i^*| = k$ . We claim that all of these assumptions can be reasonably relaxed and we empirically show that LML layers are effective in settings where these don't hold.



**Proposition 2.** *Maximizing the likelihood of  $f_\theta(x_i) : \mathcal{X} \rightarrow \mathcal{L}_k$  on only the observed data*

$$\max_{\theta} \mathbb{E} \left[ \prod_{j \in Y_i} (f_\theta(x_i))_j \right] \triangleq \mathbb{E} \left[ \prod_{j \in Y_i} P(j \in Y_i^* | x_i) \right]$$

*implicitly maximizes  $\mathbb{E}[P(Y_i^* | x_i)]$ . All expectations are done over samples from the data generating process  $(x_i, Y_i) \sim \mathcal{D}$ .*

This can be proven by observing that the model’s LML output space will allow the unobserved positive labels to have high likelihood

$$\prod_{j \in Y^* - Y} P(j \in Y^* | x)$$

while forcing all the true negative data to have low likelihood

$$\prod_{j \in \mathcal{Y} - Y^*} P(j \in Y^* | x).$$

We note that [Proposition 2](#) *does not hold* for a standard multi-label prediction model that makes predictions onto the unit hypercube  $f_\theta : \mathcal{X} \rightarrow [0, 1]^n$  where

$$\hat{p}_j = f_\theta(x_i) \triangleq P(j \in Y^* | x)$$

as only maximizing

$$\prod_{j \in Y_i} P(j \in Y^* | x)$$

will result in a collapsed model that predicts  $\hat{p}_j = 1$  for every label  $j \in \mathcal{Y}$ .

**Corollary 2.** *Maximizing the likelihood of  $f_\theta : \mathcal{X} \rightarrow \mathcal{L}_k$  on the observed data  $\mathbb{E}[P(Y_i | x_i)]$  maximizes the recall of the observed data  $\mathbb{E}[\text{recall}(Y, \hat{Y})]$ .*

The ground-truth data are vertices of the LML polytope and  $f_\theta$  approaches the ground-truth likelihoods. Thus the model’s prediction  $\hat{Y}(x)$  is the ground-truth and the recall of the observed data is maximized. We again note that the model’s 0-1 error on the observed data  $\text{error}(Y, \hat{Y})$  is in general *not* minimized, but that the error on the ground-truth data  $\text{error}(Y^*, \hat{Y})$  is minimized, as the observed data may not have all of the labels that are present in the ground-truth data.

We propose a gradient-based approach of solving this maximum likelihood problem in [Algorithm 2](#) that we use for all of our experiments.

#### 4.1 Top- $k$ Image Classification

In top- $k$  image classification, the dataset consists of images  $x_i$  with single labels  $y_i$  and the task is to predict a set of  $k$  labels  $\hat{Y}$  that maximizes  $\text{recall}(\{y_i\}, \hat{Y})$ . We show in [Section 5.2](#) that LML models are competitive with the state-of-the-art methods for top- $k$  image classification on the noisy variant of CIFAR-100 from [Berrada et al.](#).

#### 4.2 Scene Graph Generation

As briefly introduced in [Section 2.4](#), scene graph generation methods take an image as input and output a graph of the objects in the image (the nodes of the graph) and the relationships between them (the edges of the graph). One of the recent state-of-the-art methods that is characteristic of many of the other methods is Neural Motifs [[Zellers et al.](#)]. Neural Motifs and related models such as [Xu et al.](#) make an assumption that the relationships on separate edges are independent from each other. In this section, we show how we can use the maximum recall training with an LML layer to make a minor modification to the training procedure of these models that allows us to relax this assumption with negligible computational overhead.

Specifically, the Neural Motifs architecture decomposes the scene graph generation task as

$$P(G | I) = P(B | I) P(O | B, I) P(R | B, O, I)$$

where  $G$  is the scene graph,  $I$  is the input image,  $B$  is a set of region proposals, and  $O$  is a set of object proposals. The relationship generation process  $P(R | B, O, I)$  makes an independence assumption that, given a latent variable  $z$  that is present at each edge as  $z_{ij}$ , the relationships on each edge are independent. That is,

$$P([x_{i \rightarrow j}]_{ij} | z, B, O, I) = \prod_{i,j} P(x_{i \rightarrow j} | z_{ij}, B, O, I),$$

where the set of relationships between all of the nodes is  $R = [x_{i \rightarrow j}]_{ij}$ .

Neural Motifs models these probabilities with

$$P(x_{i \rightarrow j} | B, O, I) = \hat{p}_{ij} \triangleq \text{softmax}(z_{ij}) \in \Delta_n, \quad (21)$$

where  $n$  is the number of relationships for the task. The predictions are made in the  $n$ -simplex instead of the  $(n - 1)$ -simplex because an additional class is added to indicate that no relationship is present on the edge. For inference, graphs are generated by selecting the relationships that have the highest probability by concatenating all  $p_{ij}$  and selecting the top  $k$ . Typical values of  $k$  are 20, 50, and 100. The method is then evaluated on the top- $k$  recall of the scene graphs; i.e. the number of ground-truth relationships that are in the model’s top- $k$  relationship predictions.

Two drawbacks of the vanilla Neural Motif model of treating the edge relationships as independent softmax functions are that 1) edges with multiple relationships will never achieve perfect likelihood because the softmax function is being used to make a prediction at each edge. If multiple relationships are present on a single edge, the training code for Neural Motifs randomly samples a single one to use for the update in that iteration. For inference, multiple relationships on a node *can* be predicted if their individual probabilities are within the top- $k$  threshold, although they are still subject to the simplex constraints and therefore may be unreasonably low; and 2) the evaluation metric of generating a graph with  $k$  relationships is not part of the training procedure that just treats each edge as a classification problem that maximizes the likelihood of the observed relationships.

Using an LML layer to predict all of the relationship probabilities jointly overcomes these drawbacks. We model the joint probability with

$$P([x_{i \rightarrow j}]_{ij} | z, B, O, I) = \Pi_{\mathcal{L}_k}(\text{cat}([z_{ij}]_{ij})) \quad (22)$$

where  $\text{cat}$  is the concatenation function. This is now a top- $k$  recall problem that we train by maximizing the likelihood of the observed relationships with [Algorithm 2](#). We have added the LML training procedure to the official Neural Motifs codebase in  $\approx 20$  lines of code to project  $[z_{ij}]_{ij}$  onto the LML polytope instead of projecting each  $z_{ij}$  onto the simplex, and to optimize the likelihood of the data jointly instead of independently.

The LML approach for scene graph generation overcomes both of the drawbacks of the vanilla approach by 1) allowing the ground-truth data to achieve near-perfect likelihood as multiple relationships are allowed to be present between the edges, and 2) introducing the knowledge predicting  $k$  nodes into the training procedure. One downside of the LML approach for scene graph generation is that the training procedure now depends on  $k$  while the vanilla training procedure does not. We empirically show that it is typically competitive to train with a fixed  $k$  and evaluate for others.

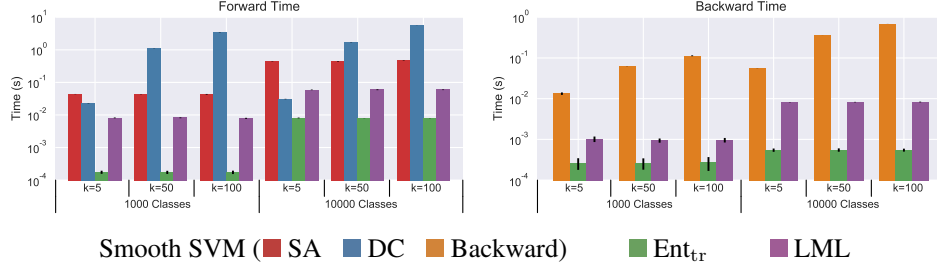


Figure 3: Timing performance results. Each point is from 50 trials on an unloaded system.

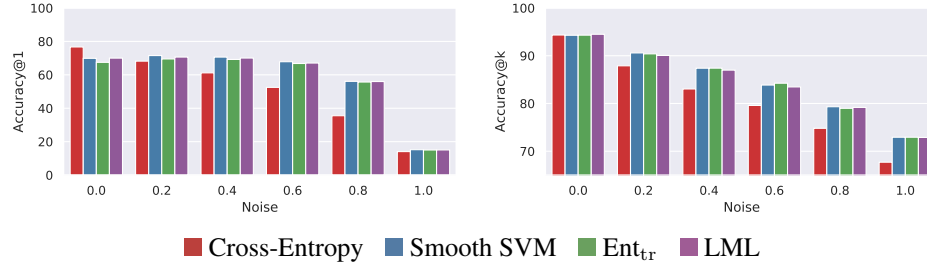


Figure 4: Testing performance on CIFAR-100 with label noise.

## 5 Experimental Results

In this section we study the computational efficiency of the LML layer and show that it performs competitively with other methods for top- $k$  image classification. When added to the Neural Motifs model for scene graph generation, LML layers improve the modeling capability with almost no computational overhead.

We have released a PyTorch implementation of the LML layer and our experimental code at

<https://github.com/locuslab/lml>

### 5.1 Performance Comparisons

The LML layer presented in [Module 1](#) has a non-trivial forward and backward pass that may be computationally expensive if not implemented efficiently. To better understand the computational costs of the LML layer, we have measured the timing performance of our layer in comparison to the Smooth SVM loss from [\[Berrada et al.\]](#) and the truncated top- $k$  entropy  $\text{Ent}_{\text{tr}}$  from [\[Lapin et al., b\]](#), which we review in [Section 2.3.1](#). The Summation Algorithm (SA) and Divide-and-Conquer (DC) algorithms for the Smooth SVM loss are further described in [Berrada et al.](#). We use the official Smooth SVM implementation and have re-implemented the truncated top- $k$  entropy in PyTorch for our experiments. The truncated top- $k$  entropy loss function is only bottlenecked by a sorting operation, which we implemented using PyTorch’s sort function.

[Figure 3](#) measures the performance of our method in comparison to the Smooth SVM and truncated top- $k$  entropy using the profiling setup from [Berrada et al.](#). We use a minibatch size of 256 and runs 50 trials for each data point. We ran all of the experiments on an unloaded NVIDIA GeForce GTX 1080 Ti GPU. The forward pass of the smooth SVM becomes computationally expensive as  $k$  grows while the LML layer’s performance and the truncated top- $k$  entropy method’s performance remain constant. The top- $k$  entropy loss is only bottlenecked by a sorting operation and significantly outperforms both the Smooth SVM and LML layers. We emphasize that [Berrada et al.](#) did not consider the truncated top- $k$  entropy method as a baseline.

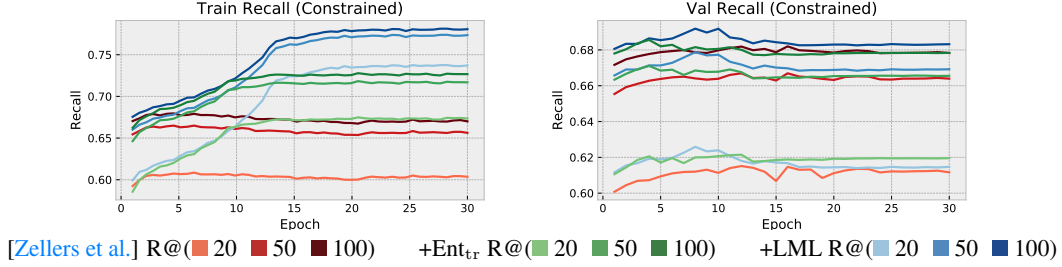


Figure 5: (Constrained) scene graph generation on the Visual Genome: Training and validation progress comparing the vanilla Neural Motif model to the  $\text{Ent}_{\text{tr}}$  and LML versions.

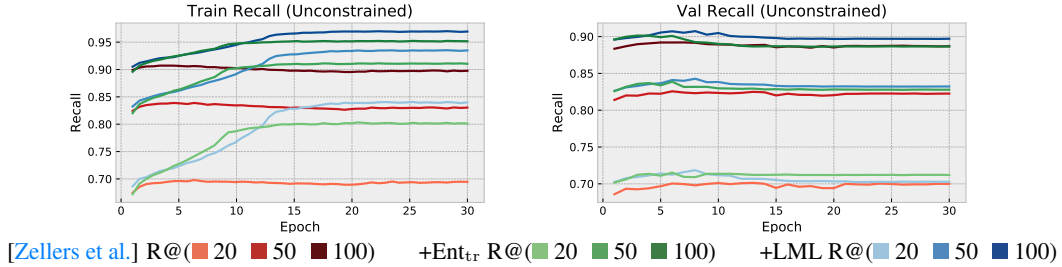


Figure 6: (Unconstrained) scene graph generation on the Visual Genome: Training and validation progress comparing the vanilla Neural Motif model to the  $\text{Ent}_{\text{tr}}$  and LML versions.

## 5.2 Top- $k$ Image Classification on CIFAR-100

We next evaluate the LML layer on the noisy top-5 CIFAR-100 task from Berrada et al. that uses the DenseNet 40-40 architecture [Huang et al.]. The CIFAR-100 labels are organized into 20 “coarse” classes, each consisting of 5 “fine” labels. With probability  $p$ , noise is added to the labels by resampling from the set of “fine” labels.

Figure 4 shows that the LML model is competitive with the other baseline methods for this task: standard cross-entropy training, the Smooth SVM models, and the truncated entropy loss. We used the experimental setup and code from Berrada et al. and added the LML experiments with a few lines of code. Notably, we also re-implemented the truncated entropy loss from Lapin et al. [b] as another reasonable baseline for this task, which Berrada et al. did not consider as a baseline. Following the method of Berrada et al., we ran four seeds for the truncated entropy and LML models and report the average test performance. For reference, a model making random predictions would obtain 1% top-1 accuracy and 5% top-5 accuracy.

The results show that relative to the cross-entropy, the smooth SVM, truncated entropy, and LML losses perform similarly. Relative to each other the best method is not clear, which is consistent with the experimental results on other tasks in Lapin et al. [b]. We interpret these results as showing that all of the methods evaluated for top- $k$  optimization learn nearly identical models despite being formulated differently.

## 5.3 Scene Graph Generation

For our scene graph generation experiments we use the MOTIFNET-LEFTRIGHT model, experimental setup, and official code from Zellers et al.. We added the LML variant with  $\approx 20$  lines of code. This experiment uses the Visual Genome dataset [Krishna et al.], using the publicly released preprocessed data and splits from Xu et al.. In this report, we focus solely on the *Predicate Classification* evaluation mode PredCls which uses a pre-trained detector and classifier and only measures improvements to the relationship predicate model  $P(R \mid B, O, I)$ . Our methods can also be extended to the other evaluation modes that jointly learn models for the detection and object classification portions  $P(G \mid I)$  and we believe that our improvements on the PredCls mode upper-bound the improvements an LML layer would add to the other evaluation modes. *Constrained* graph generation

Model	Predicate Classification (Constrained)			Predicate Classification (Unconstrained)		
	R@20	R@50	R@100	R@20	R@50	R@100
[Zellers et al.]	61.5	66.7	68.2	70.1	82.6	89.2
+LML-20	<b>62.6</b>	<b>67.9</b>	<b>69.2</b>	<b>71.9</b>	<b>84.3</b>	<b>90.7</b>
+LML-50	<b>62.5</b>	<b>67.8</b>	<b>69.1</b>	71.6	84.1	90.5
+LML-100	61.2	66.3	67.7	70.4	83.3	<b>90.7</b>
+Ent <sub>tr</sub> -20	62.1	67.1	68.6	71.5	83.9	90.1
+Ent <sub>tr</sub> -50	61.7	66.9	68.4	71.1	84.0	90.3
+Ent <sub>tr</sub> -100	60.7	66.3	67.8	69.7	83.5	90.1

Table 1: Scene graph generation on the Visual Genome: Best Validation Recall Scores

Model	Predicate Classification (Constrained)			Predicate Classification (Unconstrained)		
	R@20	R@50	R@100	R@20	R@50	R@100
[Zellers et al.]	58.5	65.2	67.1	<b>66.6</b>	<b>81.1</b>	<b>88.2</b>
+Ent <sub>tr</sub>	<b>59.4</b>	<b>66.1</b>	<b>67.8</b>	60.8	70.7	75.6
+LML	58.5	<b>66.0</b>	<b>67.9</b>	64.2	79.4	87.6

Table 2: Scene graph generation on the Visual Genome: Test Dataset Results.

constrains the graphs to have at most a single relationship present at each edge, and is more common in the literature.

We also consider using a modified version of the truncated top- $k$  entropy loss that we derive in Section 2.3.2. We do not consider modifications of the Smooth SVM because the performance results in Section 5.1 show that the approach is nearly computationally infeasible when scaling to the size necessary for scene-graph generation. An image with 20 objects and 50 possible relationships generates  $20(19)(50) = 19000$  possible relationship candidates.

All of the LML and truncated top- $k$  entropy (Ent<sub>tr</sub>) models we evaluate in this section are trained on predicting graphs with 20 relationships, which perform competitively on the validation dataset. Figure 6 shows the training progress for unconstrained graph generation. Table 1 shows the validation performance for the truncated top- $k$  entropy and LML layers when trained for  $k \in \{20, 50, 100\}$ . Figure 5 shows that the truncated top- $k$  entropy and LML approach both add representational capacity and improve the training recall by 5-10% for all evaluation modes for constrained graph generation. This behavior is also present for unconstrained graph generation in Figure 6. These improvements are not as significant on the validation dataset, or on the test dataset in Table 2. In the unconstrained evaluation mode, the LML layers outperform the truncated top- $k$  entropy and almost reach the performance of the baseline. This performance gap is likely because the Visual Genome dataset has a lot of noise from the human-generated scene graph annotations, and the LML model fits to more noise in the training dataset that does not generalize to the noise present in the validation or test datasets. Surprisingly, the LML model improves the constrained graph generation test performance but slightly decreases the unconstrained graph generation performance. We theorize this is again because of noise that the model starts to overfit to and that constraining the model to only make a single prediction at each edge is a reasonable heuristic.

## 6 Conclusions

We have presented the LML layer for top- $k$  multi-label learning. The LML layer has a forward pass that can be efficiently computed with a parallel bracketing method and a backward pass that can be efficiently computed by perturbing the KKT conditions of the optimization problem. We have empirically demonstrated that the LML layer adds representational capacity for top- $k$  optimization and in many cases can be added to existing code with  $\approx 20$  additional lines of code. As a compelling future research direction for these layers, these layers can also enable deep structured prediction models to be used for top- $k$  prediction.

## Acknowledgments

We thank Rowan Zellers for help reproducing and running the Neural Motifs training code.

## References

- Ryan Prescott Adams and Richard S Zemel. Ranking via sinkhorn propagation.
- Shivani Agarwal. The infinite push: A new support vector ranking algorithm that directly optimizes accuracy at the absolute top of the list. In *Proceedings of the 2011 SIAM International Conference on Data Mining*, pages 839–850. SIAM.
- Brandon Amos and J. Zico Kolter. Optnet: Differentiable optimization as a layer in neural networks. In *Proceedings of the International Conference on Machine Learning*.
- David Belanger and Andrew McCallum. Structured prediction energy networks.
- Leonard Berrada, Andrew Zisserman, and M Pawan Kumar. Smooth loss functions for deep top-k classification. In *Proceedings of the International Conference on Learning Representations*.
- Stephen Boyd, Corinna Cortes, Mehryar Mohri, and Ana Radovanovic. Accuracy at the top. In *Advances in neural information processing systems*, pages 953–961.
- Nataly Brukhim and Amir Globerson. Predict and constrain: Modeling cardinality in deep structured prediction.
- Amir Globerson, Nevena Lazic, Soumen Chakrabarti, Amarnag Subramanya, Michael Ringgaard, and Fernando Pereira. Collective entity resolution with multi-focal attention. In *Proceedings of the 54th Annual Meeting of the Association for Computational Linguistics (Volume 1: Long Papers)*, volume 1, pages 621–631.
- Maya R Gupta, Samy Bengio, and Jason Weston. Training highly multiclass classifiers. 15(1): 1461–1492.
- Roei Herzig, Moshiko Raboh, Gal Chechik, Jonathan Berant, and Amir Globerson. Mapping images to scene graphs with permutation-invariant structured prediction.
- Gao Huang, Zhuang Liu, Laurens Van Der Maaten, and Kilian Q Weinberger. Densely connected convolutional networks. In *2017 IEEE Conference on Computer Vision and Pattern Recognition (CVPR)*, pages 2261–2269. IEEE.
- Justin Johnson, Ranjay Krishna, Michael Stark, Li-Jia Li, David Shamma, Michael Bernstein, and Li Fei-Fei. Image retrieval using scene graphs. In *Proceedings of the IEEE conference on computer vision and pattern recognition*, pages 3668–3678.
- Ranjay Krishna, Yuke Zhu, Oliver Groth, Justin Johnson, Kenji Hata, Joshua Kravitz, Stephanie Chen, Yannis Kalantidis, Li-Jia Li, David A Shamma, et al. Visual genome: Connecting language and vision using crowdsourced dense image annotations. 123(1):32–73.
- Maksim Lapin, Matthias Hein, and Bernt Schiele. Top-k multiclass svm. In *Advances in Neural Information Processing Systems*, pages 325–333, a.
- Maksim Lapin, Matthias Hein, and Bernt Schiele. Loss functions for top-k error: Analysis and insights. In *Proceedings of the IEEE Conference on Computer Vision and Pattern Recognition*, pages 1468–1477, b.
- Nan Li, Rong Jin, and Zhi-Hua Zhou. Top rank optimization in linear time. In *Advances in neural information processing systems*, pages 1502–1510, a.
- Yikang Li, Wanli Ouyang, Bolei Zhou, Jianping Shi, Chao Zhang, and Xiaogang Wang. Factorizable net: an efficient subgraph-based framework for scene graph generation. In *European Conference on Computer Vision*, pages 346–363. Springer, b.

- Xiaodan Liang, Lisa Lee, and Eric P Xing. Deep variation-structured reinforcement learning for visual relationship and attribute detection. In *Computer Vision and Pattern Recognition (CVPR), 2017 IEEE Conference on*, pages 4408–4417. IEEE.
- Li-Ping Liu, Thomas G Dietterich, Nan Li, and Zhi-Hua Zhou. Transductive optimization of top k precision.
- Andre Martins and Ramon Astudillo. From softmax to sparsemax: A sparse model of attention and multi-label classification. In *International Conference on Machine Learning*, pages 1614–1623.
- Gonzalo Mena, David Belanger, Scott Linderman, and Jasper Snoek. Learning latent permutations with gumbel-sinkhorn networks.
- Alejandro Newell and Jia Deng. Pixels to graphs by associative embedding. In *Advances in neural information processing systems*, pages 2171–2180.
- Vlad Niculae, André FT Martins, Mathieu Blondel, and Claire Cardie. Sparsemap: Differentiable sparse structured inference.
- Bryan A Plummer, Arun Mallya, Christopher M Cervantes, Julia Hockenmaier, and Svetlana Lazebnik. Phrase localization and visual relationship detection with comprehensive image-language cues. In *Proc. ICCV*.
- Alain Rakotomamonjy. Sparse support vector infinite push.
- David Raposo, Adam Santoro, David Barrett, Razvan Pascanu, Timothy Lillicrap, and Peter Battaglia. Discovering objects and their relations from entangled scene representations.
- Jean-Charles Régin. Generalized arc consistency for global cardinality constraint. In *Proceedings of the thirteenth national conference on Artificial intelligence-Volume 1*, pages 209–215. AAAI Press.
- Cynthia Rudin. The p-norm push: A simple convex ranking algorithm that concentrates at the top of the list. 10(Oct):2233–2271.
- Rodrigo Santa Cruz, Basura Fernando, Anoop Cherian, and Stephen Gould. Visual permutation learning.
- Daniel Tarlow, Kevin Swersky, Richard S Zemel, Ryan Prescott Adams, and Brendan J Frey. Fast exact inference for recursive cardinality models.
- Sanghyun Woo, Dahun Kim, Donghyeon Cho, and In So Kweon. Linknet: Relational embedding for scene graph. In *Advances in Neural Information Processing Systems*, pages 558–568.
- Danfei Xu, Yuke Zhu, Christopher B Choy, and Li Fei-Fei. Scene graph generation by iterative message passing. In *Proceedings of the IEEE Conference on Computer Vision and Pattern Recognition*, volume 2.
- Michael Ying Yang, Wentong Liao, Hanno Ackermann, and Bodo Rosenhahn. On support relations and semantic scene graphs. 131:15–25.
- Rowan Zellers, Mark Yatskar, Sam Thomson, and Yejin Choi. Neural motifs: Scene graph parsing with global context. In *Proceedings of the IEEE Conference on Computer Vision and Pattern Recognition*, pages 5831–5840.